Multiplex gene editing models of del(7q) reveal combined *CUX1* and *EZH2* loss drives clonal expansion and drug resistance

Matthew R. M. Jotte,[1-3] Angela Stoddart,[2,4] Tanner C. Martinez,[1,2,5] Raven Moten,[2,6] Yuqing Xue,[2,3] Molly K. Imgruet,[1-3] Hunter Blaylock,[2,3] Henna S. Nam,[2] Bonnie Hu,[2] Jermaine Austin,[3] Ningfei An,[2] Saira Khan,[2] Sandeep K. Gurbuxani,[2,7] and Megan E. McNerney[2-4,7]

[1]Interdisciplinary Scientist Training Program, [2]Department of Pathology, [3]Committee on Cancer Biology, [4]Department of Pediatrics, [5]Committee on Immunology, [6]Committee on Genetics, Genomics, and Systems Biology, and [7]The University of Chicago Medicine Comprehensive Cancer Center, The University of Chicago Medicine, Chicago, IL

Key Points

- Multiplex gene knockout is a tractable technique to model aneuploid events.

- Combined loss of the 7q genes *CUX1* and *EZH2* impairs the DNA damage response, driving hematopoietic clonal expansion and drug resistance.

Loss of all or part of chromosome 7 [−7/del(7q)] is recurrent in myeloid neoplasms and associated with a poor response to chemotherapy. Chromosome 7–encoded genes driving drug resistance and the consequences of combinatorial 7q tumor suppressor gene loss have remained unclear, the latter question largely because of the challenges of modeling aneuploidy. Here, we use in silico data mining to uncover 7q genes involved in chemotherapy resistance. We establish murine models of del(7q) clonal hematopoiesis and drug resistance with multiplex CRISPR-Cas9 (CRISPR–associated protein 9)–mediated inactivation of 4 genes, *Cux1*, *Ezh2*, *Kmt2c*, and *Kmt2e*. Postgenotoxic exposure, combined deficiency of *Cux1* and *Ezh2* preferentially promotes clonal myeloid expansion in vivo, with compounding defects in DNA damage recognition and repair. Human acute myeloid leukemia cell lines similarly illustrate central roles for *CUX1* and *EZH2* loss in survival and DNA damage resolution after chemotherapy exposure. Transcriptome analysis reveals combined *Cux1* and *Ezh2* loss recapitulates gene signatures of -7 patients and defective DNA damage response pathways, to a greater extent than single gene loss. This work reveals a genetic interaction between *CUX1* and *EZH2*, and sheds light on how −7/del(7q) contributes to leukemogenesis and drug resistance characteristic of these adverse-risk neoplasms. These data support the concept of 7q as a contiguous gene syndrome region, in which combined loss of multiple gene drives pathogenesis. Furthermore, our CRISPR-based approach may serve as a framework for interrogating other recurrent aneuploid events in cancer.

Introduction

Aneuploid karyotypes are prevalent in human cancers, with >90% of solid and 75% of hematopoietic malignancies deviating from 46 chromosomes.[1] Large-scale gain or loss of chromosomal material increase or decreases the dosage all encoded genes, affecting multiple cellular processes including protein homeostasis, metabolism, and proliferation.[2-4] Despite this pervasiveness, the pathogenesis of

The full-text version of this article contains a data supplement.

recurrent aneuploidies remains largely unclear, in part due to a paucity of model systems. Isolated aneuploidies, particularly monosomies, are challenging to generate and often unstable in culture systems,[5,6] and lack of chromosomal synteny between humans and animal species hinders development of animal models.[5,7,8]

Loss of all or part of chromosome 7 [−7/del(7q)] is recurrent in high-risk myeloid malignancies, including pediatric and adult myelodysplastic syndrome and acute myeloid leukemia (AML), and associated with poor prognosis.[9-11] Strikingly, −7/del(7q) occurs in up to 50% of therapy-related myeloid neoplasms (t-MNs), also referred to as myeloid neoplasms post-cytotoxic therapy, high-risk malignancies that arise after radiation or chemotherapy exposure.[12-14] Recently, chromosomal alterations have been identified in clonal hematopoiesis (CH), and del(7q) CH is associated with increased risk of developing myeloid disease.[15-18] CH is also associated with subsequent t-MN,[19,20] suggesting that a preexisting clonal population harboring −7/del(7q) is selected for by radiation and/or chemotherapy, expands, and transforms to t-MN. This etiology may also contribute to drug resistance in t-MN, because the initiating population has already undergone selection under genotoxic pressure.[7]

Multiple candidate tumor suppressor genes (TSGs) have been identified within commonly deleted regions (CDRs) of 7q.[7,21-23] Our laboratory identified the homeobox transcription factor *CUX1*, encoded in the 7q22 CDR, as a potent haploinsufficient TSG.[24] *Cux1* deficiency induces myelodysplastic syndrome with lethal anemia, and *Cux1*-deficient cells are rapidly selected for after alkylating agent exposure and establish t-MNs, demonstrating that even this single 7q gene deficiency can drive disease development.[25-27] However, additional 7q TSGs have hematopoietic deletion phenotypes, and the effects, if any, of combinatorial 7q gene deletions on disease pathogenesis and drug resistance remain unclear.

In this study, we develop a murine model of del(7q) CH and drug resistance by simultaneously inactivating up to 4 7q candidate TSGs (*Cux1*, *Ezh2*, *Kmt2c*, and *Kmt2e*) in hematopoietic stem cells (HSCs) using multiplex CRISPR-Cas9 (CRISPR–associated protein 9) editing. We observe significant myeloid expansion of clones edited for *Cux1* and *Ezh2*, which is accelerated upon chemotherapy exposure. *Cux1;Ezh2*-deficient cells also display reduced sensitivity to the AML therapeutic daunorubicin, linking these 7q genes to the drug resistance characteristic of t-MNs. Mechanistically, *Cux1;Ezh2*-deficient cells have profoundly impaired DNA double-strand break recognition and repair after genotoxic stress, driving drug resistance and clonal expansion.

Methods

In silico data mining

Nine genome-wide CRISPR knockout screens for resistance against cisplatin, etoposide, or doxorubicin were downloaded from the BioGRID ORCS (Biological General Repository for Interaction Datasets Open Repository of CRISPR Screens) database.[28-37] For each screen, we identified genes in which targeting guide RNAs (gRNAs) had positive z-scores, indicating increased drug resistance after gene deletion, then narrowed to chromosome 7 genes expressed in human HSCs and located in 7q CDRs.[25] We entered the final list of 39 candidates into the Molecular Signatures Database to identify relevant functional pathways.[38]

Multiplex CRISPR-Cas9 knockout in HSPCs

CRISPR gRNAs were designed by intersecting top hits from the Synthego and Broad Institute gRNA design tools. Cas9:gRNA ribonucleoprotein complexes (RNPs) were assembled by mixing gRNA with Cas9-2NLS protein (Synthego Corp [Redwood City, CA]) to 3:1 molar ratio and incubating at room temperature for 15 to 30 minutes.[39] Donor c-kit[+] hematopoietic stem and progenitor cells (HSPCs) were isolated and transfected with RNPs using the NEON transfection system (Thermo Fisher Scientific [Waltham, MA]) at 1900 volts, 20-millisecond duration, 1 pulse.

Tracking gene knockout in the peripheral blood

After HSPC engraftment, peripheral blood was routinely collected from the submandibular vein of recipient mice. DNA was isolated from mononuclear cells after red cell depletion using the Wizard Genomic DNA Purification kit (Promega Corp [Madison, WI]). The genomic region flanking the gRNA cut site was polymerase chain reaction amplified. Sanger sequencing traces were aligned using Synthego's CRISPR edits tool to determine gene knockout efficiencies.

Results

In silico data mining identifies chromatin modifiers as candidate 7q genes modulating drug resistance

Our laboratory previously demonstrated that CUX1 regulates chemotherapy resistance and epigenetic-driven DNA repair.[26] To identify additional chromosome 7 genes modulating resistance, we mined 9 genome-wide CRISPR-Cas9 knockout screens available on BioGRID for resistance to etoposide and cisplatin, chemotherapeutics associated with t-MN development, and anthracyclines, used to treat de novo AML and t-MN.[7] Within each screen, we identified any chromosome-7 genes in which targeting gRNAs were enriched in drug-treated cells compared with vehicle, then limited the list to genes expressed in CD34^{+} HSPCs (113 genes). We retained genes within 7q CDRs, yielding 39 candidates (supplemental Table 1). Pathway analysis demonstrated significant enrichment for transcriptional coregulators and chromatin-modifying enzymes, notably the histone modifiers *EZH2*, *KMT2C/MLL3*, and *KMT2E/MLL5* (Figure 1A). Loss of *EZH2*, encoding the catalytic component of the H3K27 methyltransferase Polycomb Repressive Complex 2 (PRC2),[40,41] is associated with resistance to anthracyclines and poor prognosis in AML, validating our in silico approach.[42] Heterozygosity of *KMT2C*, a component of the COMPASS complex that catalyzes H3K4 monomethylation,[43,44] promotes resistance to alkylating agents in HSCs.[45] Inactivating *KMT2C* mutations are also observed in relapsed pediatric AML, further supporting a role in chemotherapy resistance.[46] Loss of *KMT2E*, also part of the KMT/MLL (lysine methyltransferase/mixed lineage leukemia) family, impairs HSC function,[47-49] and decreased *KMT2E* expression is associated with worse outcomes in AML.[50]

KMT2C, *KMT2E*, and *EZH2* are among the highest expressed 7q candidates in human HSPCs (Figure 1A) and have each been reported to mediate DNA repair.[51-55] Despite megabase distances between these genes, they are collectively lost in >70% of patients with −7/del(7q) based on copy-number analysis of 2 patient cohorts[24,56] (Figure 1B). Therefore, we surmised that these genes are appropriate candidates to examine drug resistance and genetic interaction with *CUX1* loss.
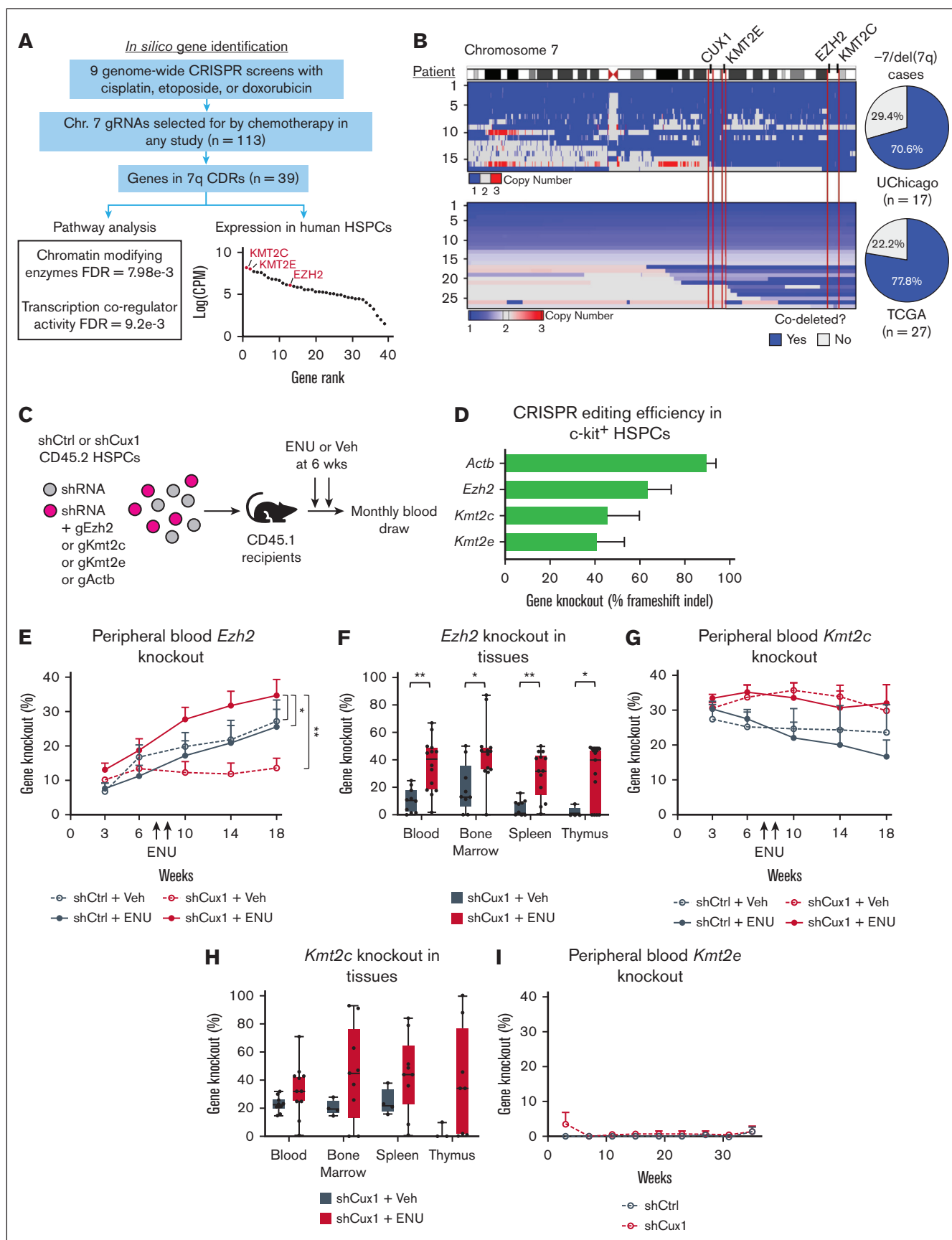
Figure 1.

Combined *Cux1* and *Ezh2* deficiency promotes hematopoietic expansion after exposure to alkylating agents

Our laboratory reported that *Cux1*-deficient cells outcompete wild-type cells after exposure to the DNA-damaging alkylating agent N-ethyl-N-nitrosourea (ENU).[26] To test additional 7q gene deficiencies, we used an RNP-based CRISPR-Cas9 delivery method[39] to knock out *Ezh2*, *Kmt2c*, or *Kmt2e* in HSPCs (Figure 1C; supplemental Figure 1A). This approach yields polyclonal populations with high levels of insertions and deletions detectable within 72 hours after transfection (Figure 1D; supplemental Figure 1B-C). We reasoned that the additive effects of combinatorial gene deletion would be most accurately uncovered by chemotherapy pressure in vivo. As such, we RNP-transfected CD45.2 HSPCs derived from our transgenic mouse models harboring a doxycycline-inducible short hairpin RNA targeting *Cux1* (shCux1) or renilla luciferase as a control (shCtrl).[25] Lethally irradiated CD45.1 transplant recipients were maintained on doxycycline. As ENU is the only chemotherapeutic reported to cause t-MN in mice,[57,58] we injected recipient mice with ENU (100 mg/kg) or vehicle to model chemotherapy exposure and tracked gene knockout in the peripheral blood, defined as the sum of frameshift indel frequencies. We detected gene knockout beyond 16 weeks after transplant, indicating successful editing of long-term HSCs.[59]

We observed significant expansion of *Ezh2* knockout but not control *Actb* insertions and deletions[60] (supplemental Figure 1D) in ENU-treated mice receiving shCux1 HSPCs (Figure 1E). We also detected significantly increased *Ezh2* knockout in other hematopoietic tissues of ENU-treated shCux1 recipients (Figure 1F), further demonstrating increased selection for combined *Cux1*;*Ezh2* deficiency over *Cux1* deficiency alone. In mice given shCtrl HSPCs there was a general increase in *Ezh2* knockout over time, but ENU administration did not affect expansion in the peripheral blood or other tissues (Figure 1E; supplemental Figure 1E). Bone marrow *Ezh2* knockout approached 90% in some ENU-treated mice, consistent with expansion of cells with biallelic *Ezh2* loss (Figure 1F; supplemental Figure 1F), which has been observed in −7/del(7q) patients.[17,61]

In contrast to *Ezh2*, we did not observe selection for *Kmt2c* knockout in the peripheral blood after ENU exposure (Figure 1G).

We did detect increased *Kmt2c* knockout in other hematopoietic tissues of ENU-treated shCux1 recipients (Figure 1H) but not shCtrl-treated recipients (supplemental Figure 1G). *Kmt2e*-null cells reportedly fail to engraft after transplant,[48] and we also noted low peripheral blood *Kmt2e* knockout (Figure 1I) despite detectable knockout after transfection and successful CD45.2 engraftment (supplemental Figure 1H). However, we did observe increased bone marrow *Kmt2e* knockout in some shCux1 mice compared with shCtrl-treated mice (supplemental Figure 1I). Overall, we demonstrate strong selection for combined *Cux1*;*Ezh2* deficiency and potential selection for *Cux1*;*Kmt2c* deficiency under genotoxic stress.

Multiplex 7q gene knockout in HSCs indicates that combined *Cux1* and *Ezh2* deficiency primarily drives expansion after chemotherapy exposure

Next, we transfected shCtrl and shCux1 HSPCs with RNPs targeting *Ezh2*, *Kmt2c*, and *Kmt2e* simultaneously (Figure 2A). To ensure that the low engraftment of *Kmt2e*-null cells was not due to off-target effects, we used a second *Kmt2e* gRNA targeting a different exon in these experiments (supplemental Figure 1A). Genotyping colonies from individual HSPCs revealed that this multiplex knockout approach is efficient, with 75% of colonies containing edits, and 60% showing perturbations to all 3 genes (Figure 2B). Furthermore, we observed both monoallelic and biallelic knockout, enabling modeling of monosomy and recapitulating the biallelic *EZH2* and *KMT2C* mutations detected in patients.[23,62]

We reasoned that the knockout combination with the highest fitness should be selected for and expanded. We transplanted multiplex-edited shCtrl or shCux1 CD45.2 HSPCs into CD45.1 recipients, maintained recipients on doxycycline, and treated mice with ENU or vehicle to model chemotherapy exposure. Input knockout of all genes was comparable between shCtrl- and shCux1-edited cells for both vehicle- and ENU-treated cohorts. At a population level, knockout frequencies were stable within the vehicle-treated mice (Figure 2C) with some exceptions characterized hereafter. In contrast, ENU exposure accelerated expansion of *Ezh2* knockout in all mice, with shCux1 recipients showing significantly higher *Ezh2* knockout than shCtrl recipients across 40 weeks (Figure 2D). ENU-treated shCux1 recipient mice also displayed expansion of peripheral blood myeloid cells that significantly correlated with *Ezh2* knockout levels (Figure 2E), and

---

Figure 1. Combined deficiency of *Cux1* and *Ezh2* is selected for after alkylating agent exposure. (A) Nine genome-wide screens were analyzed to identify Chr 7 genes that promote resistance to chemotherapy when inactivated. Pathway analysis and RNA expression in human HSPCs is shown in counts per million. (B) Copy-number analysis of Chr 7 from 2 patient cohorts from UChicago and TCGA. The regions encoding *CUX1*, *KMT2E*, *KMT2C*, and *EZH2* are denoted in red, and the percentage of −7/del(7q) patients with deletion of all 4 genes is shown. (C) Experimental scheme for pairwise-knockout transplant cohorts. shCtrl and shCux1 c-kit⁺ HSPCs were transfected with RNPs targeting *Ezh2*, *Kmt2c*, *Kmt2e*, or an intron of *Actb* and transplanted into wild-type recipients. Two doses of ENU (100 mg/kg) were administered intraperitoneally, 9 days apart, beginning 6 weeks after transplant. (D) 7q gene knockout percentages, defined as the sum of frameshift insertions and deletions (indels), after RNP transfection. Total indels, including those in-frame, are plotted for *Actb* as the gRNA targets an intron (n = 4 trials for *Actb*, n = 15 for *Ezh2*, n = 17 for *Kmt2c*, and n = 14 for *Kmt2e*). Data are plotted as mean + standard deviation (SD). (E) *Ezh2* gene knockout was serially tracked in peripheral blood mononuclear cells by Sanger sequencing before and after vehicle (Veh) or ENU administration. Data are plotted as mean + standard error of the mean (SEM), and 2 independent biological replicates were performed with 5 to 7 mice per replicate per genotype, for a total of 10 to 14 mice per experimental group. Significance from a 2-way analysis of variance (ANOVA) is shown. *$P < .05$; **$P < .01$. (F) Box plots of *Ezh2* knockout in hematopoietic tissues at euthanasia of Veh- or ENU-treated shCux1 recipient mice, 18 to 22 weeks after transplant (n = 10-13 mice). Significance from a 2-tailed *t* test is shown. *$P < .05$; **$P < .01$. (G) *Kmt2c* knockout was tracked as in panel E for Veh- and ENU-treated recipients. Data are plotted as mean + SEM, and 2 independent biological replicates were performed with 4 to 6 mice per replicate per genotype, for a total of 9 to 11 mice per experimental group. (H) Box plots of *Kmt2c* knockout in hematopoietic tissues at euthanasia as in panel F (n = 3-11 mice). (I) *Kmt2e* knockout was tracked as in panels E,G for 36 weeks (n = 5 mice per experimental group). CPM, counts per million; Chr 7, chromosome 7; FDR, false discovery rate; TCGA, The Cancer Genome Atlas Program; UChicago, The University of Chicago.
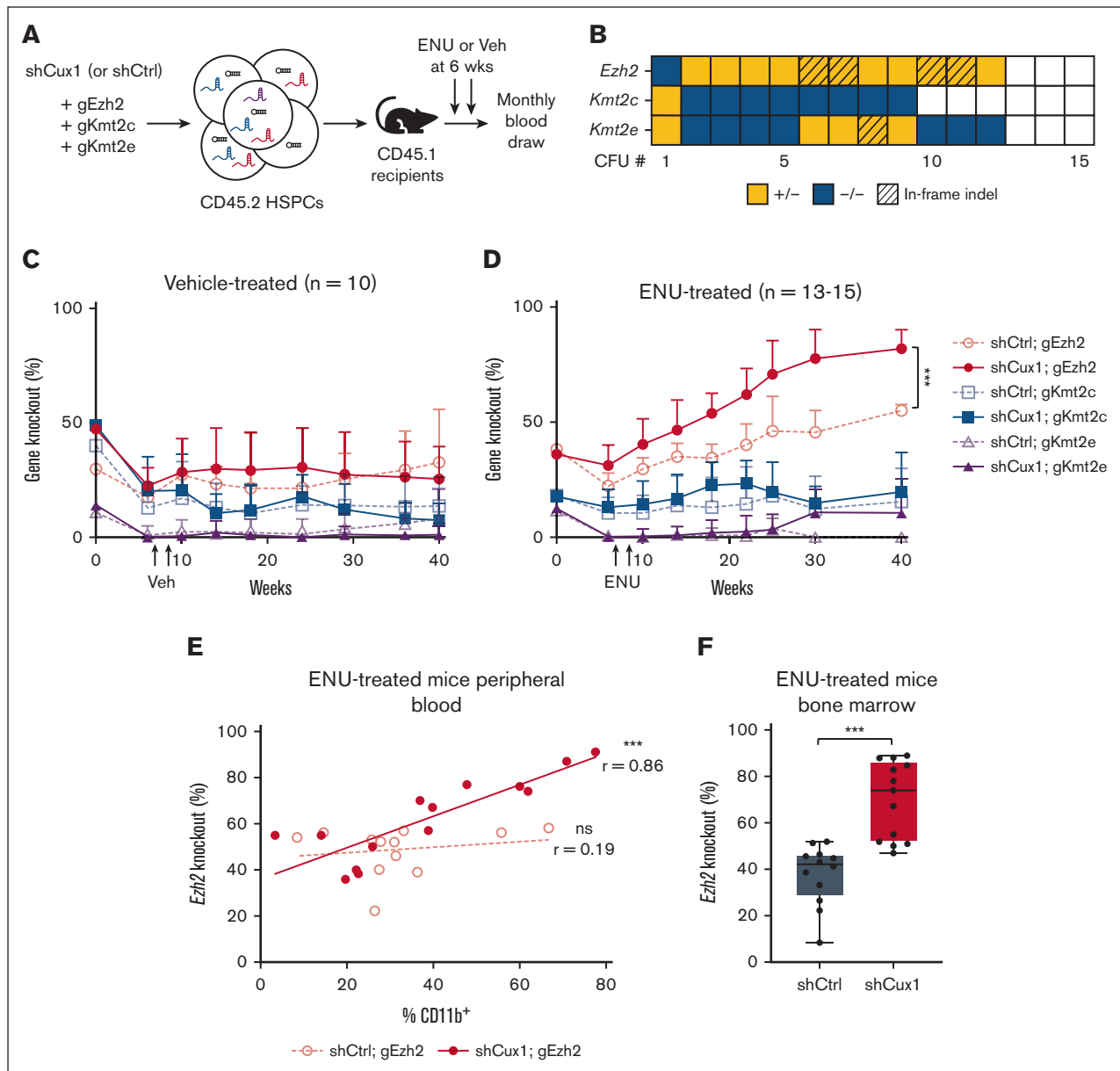
Figure 2. Multiplex knockout of 7q genes in HSCs indicates combined *Cux1;Ezh2* deficiency drives expansion after chemotherapy exposure. (A) Experimental schematic for multiplex knockout transplant cohorts. shCtrl and shCux1 c-kit⁺ HSPCs were transfected with a pool of RNPs targeting *Ezh2*, *Kmt2c*, and *Kmt2e* to generate mosaic populations of cells harboring different combinations of 7q gene knockout. Two doses of ENU were administered to recipient mice (100 mg/kg) 9 days apart, beginning 6 weeks after transplant. (B) Transfected HSPCs were plated in MethoCult M3434, cultured for 7 to 10 days, and colonies derived from individual cells were genotyped. Each column represents data from 1 colony. Blue shading denotes homozygous knockout, yellow denotes heterozygous knockout, and hatched lines denote the second allele harbored an in-frame indel that does not cause a frameshift. Fifteen colonies were analyzed across 2 independent multiplex transfections. (C) Gene knockout frequencies were serially tracked in the peripheral blood of transplant recipients before and after Veh administration. Data are plotted as mean + SD, total 10 mice receiving multiplex-edited shCtrl or shCux1 cells. (D) Gene knockout frequencies in the peripheral blood as in panel C, for mice given ENU. Data are plotted as mean + SD, total 13 to 15 mice receiving multiplex-edited shCtrl or shCux1 cells. Significance from a 2-way ANOVA is shown. ***$P < .001$. (E) The percent of CD11b⁺ myeloid cells (x-axis) and *Ezh2* knockout (y-axis) in the peripheral blood of ENU-treated recipients at euthanasia. CD11b positivity was assessed by flow cytometry. Simple linear regression was performed to fit a line to the data, and significance from Pearson *r* is shown. ***$P < .001$. (F) Box plots showing total *Ezh2* knockout in the bone marrow of ENU-treated recipients at euthanasia. Significance from a 2-tailed *t* test is shown. ***$P < .001$. CFU, colony-forming unit; ns, not significant.

significantly higher bone marrow *Ezh2* knockout (Figure 2F). These data again demonstrate prominent selection for combined *Cux1*-*Ezh2* deficiency.

Individual mice inform the consequences of 7q gene loss on clonal expansion

In recipients of multiplex-edited shCtrl HSPCs, 70% (7/10) of vehicle-treated mice showed stable knockout scores for *Ezh2*, *Kmt2c*, and *Kmt2e* for the duration of the study. In 30% (3/10), we observed successive increases in *Ezh2*, *Kmt2c*, and *Kmt2e* knockout (Figure 3A). Mouse 391 was euthanized early due to anal prolapse but displayed rapid increases in knockout for all 3 7q genes. In mouse 392 and mouse 458, the steady knockout increase after 20 weeks suggests an HSC with combinatorial loss of these epigenetic regulators had a clonal advantage independent of *Cux1* loss. In the bone marrow of mouse 458, we observed a major clone with biallelic *Ezh2* and monoallelic *Kmt2e* knockout (Figure 3B). *Kmt2e* knockout was not detected early, suggesting an *Ezh2*$^{-/-}$;*Kmt2e*$^{+/-}$ HSC existed after transplant but only gained a clonal advantage through aging.

For recipients of multiplex-edited shCux1 HSPCs, 70% (7/10) of vehicle-treated mice also displayed stable knockout scores. The remaining 30% (3/10) of mice developed malignancies under 24 weeks (Figure 3C), not seen in the shCtrl cohort. These mice displayed concurrent increases in total white blood cells and decreases in red blood cells, and increased peripheral blood neutrophils and decreased lymphocytes (supplemental Figure 2A-B). Mouse 442 contained a high percent of Gr1$^+$Cd11b$^+$ myeloid cells in the bone marrow and spleen (81% and 46%, respectively) and individual bone marrow–derived colony analysis showed *Cux1*-deficient clones with heterozygous *Ezh2* knockout, alone and in combination with *Kmt2c* or *Kmt2e* (Figure 3D). Secondary transplants from mouse 441 and 466 confirmed that the major malignant clones in these mice were of T-cell origin (supplemental Figure 2C). These vehicle-treated cohorts provide proof-of-principle that combinatorial loss of multiple 7q genes can promote clonal expansion at low frequency and long latency.

The rate of expansion with *Cux1* deficiency was most clearly seen with ENU administration (Figure 2D). ENU is known to induce murine thymic lymphomas,[63] and most of our mice succumbed to lymphoma regardless of genotype. However, 31% (4/13) and 27% (4/15) of recipients of multiplex-edited shCtrl and shCux1 HSPCs, respectively, did not develop thymic lymphomas; all 8 mice presented with progressive anemia and splenomegaly at euthanasia (Figure 3E-F). The effacement of splenic architecture, granulocytosis, and monocytosis were more severe in shCux1 recipients (Figure 3G; supplemental Figure 2D). At euthanasia, peripheral blood *Ezh2* knockout approached 100% in shCux1 recipients (74%-91%) and ranged from 39% to 57% in shCtrl recipients (Figure 3H). Most bone marrow clones in shCux1 recipients had biallelic *Ezh2* knockout (supplemental Figure 2E), suggesting *Cux1* loss and stress positively select for complete *Ezh2* inactivation.

We detected similar frequencies of Lin$^-$Sca-1$^+$c-kit$^+$ HSPCs in these 8 ENU-treated mice (supplemental Figure 3A) suggesting the increase in *Ezh2* knockout was not simply due to a larger total stem and progenitor cell pool. To test whether the cells retain sensitivity to ENU, we performed secondary transplants and treated recipients with ENU or vehicle to model a second wave of chemotherapy (supplemental Figure 3B). Only recipients of shCux1 primary samples expanded after repeat ENU administration, showing increased peripheral blood CD45.2 levels and bone marrow *Ezh2* knockout (supplemental Figure 3C-D). Of note, we still observed similar levels of Lin$^-$Sca-1$^+$c-kit$^+$ HSPCs and myeloid progenitors in secondary shCtrl and shCux1 recipients (supplemental Figure 3E). This latter finding suggests that although the total number of HSPCs remains unchanged, the proportion of *Ezh2*-edited shCux1 cells expanded within that pool. ENU does not induce a strong proliferative effect on HSPCs despite reducing marrow cellularity, in contrast to other compounds such as 5-fluorouracil (supplemental Figure 3F-G), suggesting that combined *Cux1*;*Ezh2* deficiency contributes to expansion primarily through chemotherapy resistance.

Kmt2c loss associates with, but does not drive, expansion of *Ezh2*- or *Cux1*;*Ezh2*-deficient clones

Although all primary ENU-treated mice displayed peripheral blood *Ezh2* knockout expansion, some showed simultaneous *Ezh2* and *Kmt2c* knockout expansion. An example of concurrent expansion is given in Figure 4B (comparison in Figure 4A). We reasoned that the expanding clones in mice with significantly correlated *Ezh2*/*Kmt2c* knockout harbored inactivation of both genes (supplemental Figure 4A). Genotyping individual bone marrow–derived colonies confirmed that these mice had dominant clones with both *Ezh2* and *Kmt2c* knockout; in contrast, mice with uncorrelated peripheral blood *Ezh2*/*Kmt2c* knockout had no colonies with concurrent knockout (Figure 4C-D).

We analyzed whether clones with concurrent *Ezh2* and *Kmt2c* loss had greater expansion after ENU exposure than those with only *Ezh2* loss. We compared maximum *Ezh2* and *Kmt2c* knockout values between mice with and without significantly correlated *Ezh2*/*Kmt2c* knockout trajectories as a measure of greatest expansion. In both shCtrl and shCux1 recipients, maximum *Kmt2c* knockout was almost twofold higher in correlated (concurrent) vs uncorrelated *Ezh2*/*Kmt2c* knockout (Figure 4E). In shCtrl recipients, *Ezh2* knockout remained at ~50% regardless of correlation with *Kmt2c* knockout, suggesting *Kmt2c* is a passenger mutation in these clones and has no influence on the dynamics of *Ezh2* expansion (Figure 4F). In contrast, there was a trend ($P = .066$) toward higher *Ezh2* knockout in shCux1 recipients with correlated *Ezh2*/*Kmt2c* knockout (Figure 4F). As a second metric, we compared the slopes of *Ezh2* and *Kmt2c* knockout expansion in mice with and without correlated expansion (supplemental Figure 4B). This analysis also trended toward faster expansion in mice with combined *Cux1*;*Ezh2*;*Kmt2c* deficiency compared with *Cux1*;*Ezh2* alone ($P = .08$). Collectively, our data suggest that *CUX1* and *EZH2* loss primarily influence −7/del(7q) clonal expansion and t-MN development, although it is possible that there are additional unmeasured mutations from ENU mutagenesis. Nonetheless, the association of *Kmt2c* knockout with *Cux1*;*Ezh2* deficiency may have progressive consequences on malignancy.

CUX1;*EZH2* deficiency promotes resistance to the MN therapeutic daunorubicin

Because t-MNs are often drug resistant, we generated heterozygous single-cell CRISPR knockout clones in U937 human myeloid leukemia cells for each 7q gene (Figure 5A) and tested for increased resistance to the anthracycline daunorubicin, a core
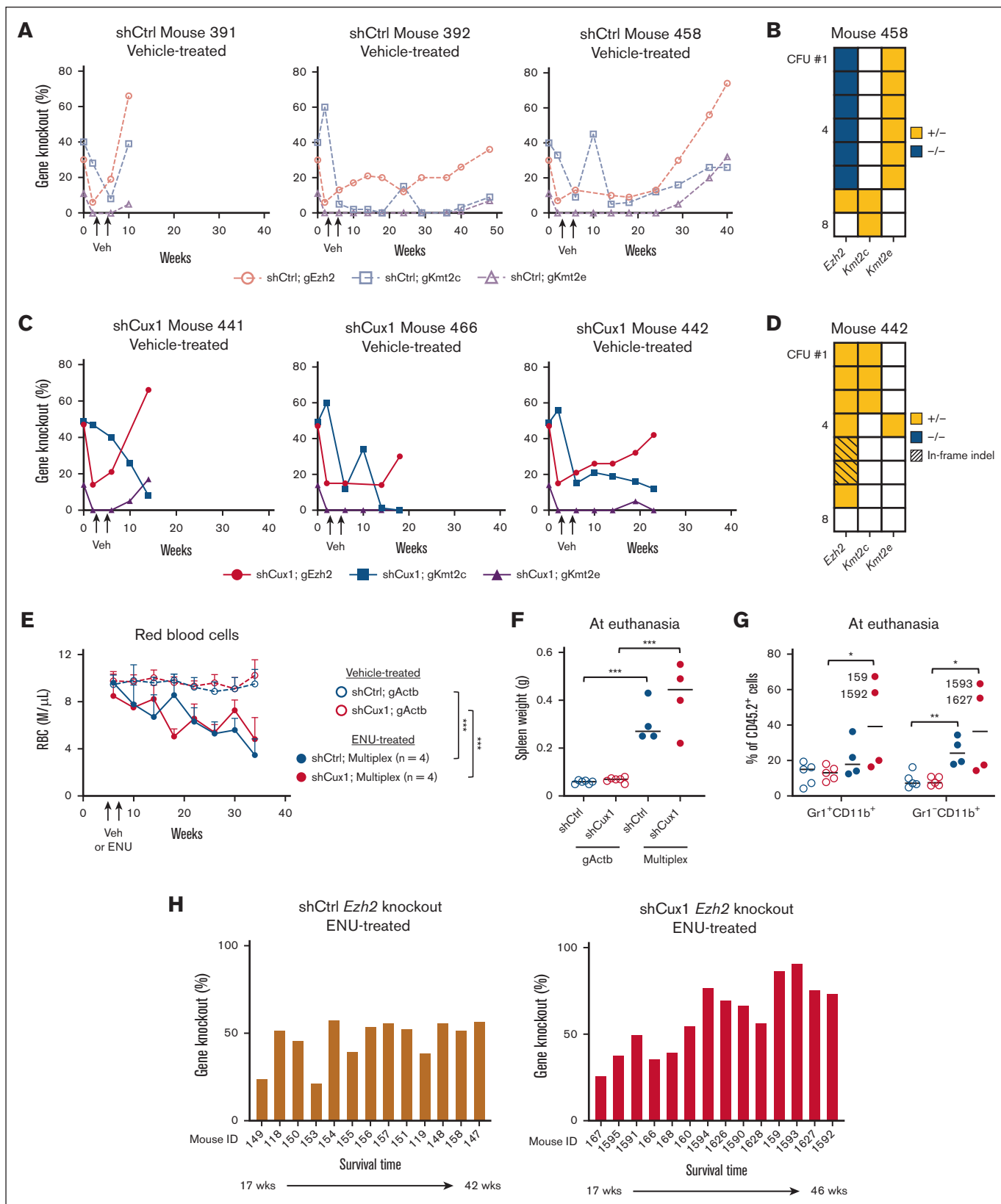
Figure 3. *Cux1* loss accelerates clonal expansion and selection for biallelic *Ezh2* loss. (A) Peripheral blood gene knockout frequencies of 3 Veh-treated recipients of multiplex-edited shCtrl HSPCs that demonstrated knockout expansion over time. (B) Bone marrow cells from shCtrl mouse 458 were plated in MethoCult M3434 methylcellulose, cultured for 1 week, and colonies derived from individual cells were genotyped. Each row represents data from 1 colony. Blue shading denotes homozygous knockout, and yellow shading denotes heterozygous knockout. (C) Gene knockout frequencies as in panel A for 3 Veh-treated recipients of multiplex-edited shCux1 HSPCs that demonstrated knockout expansion over time. (D) Genotyping of colonies as in panel B from bone marrow of shCux1 mouse 442. Each row represents data from 1 colony. (E) Total RBC count
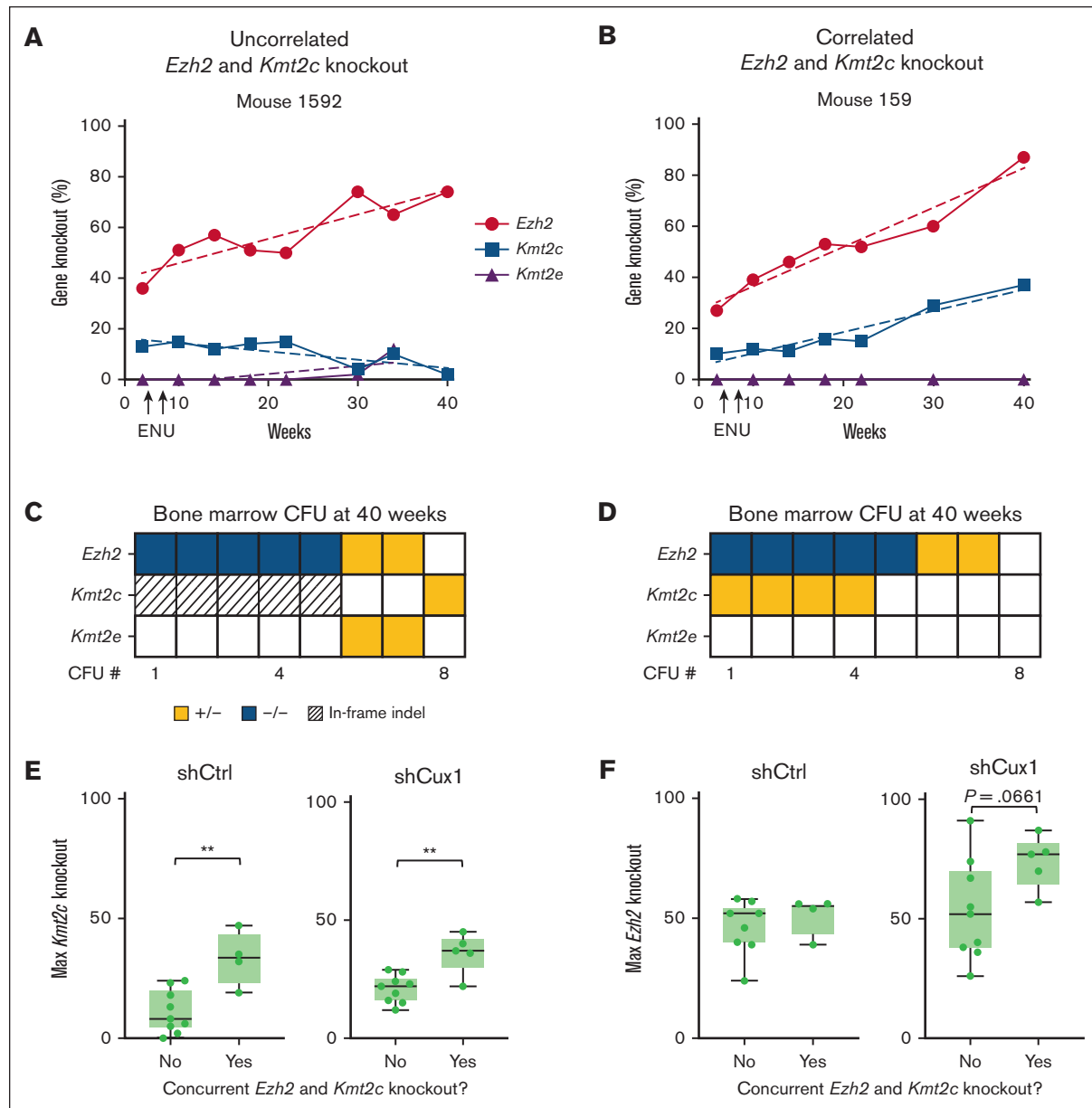
Figure 4. *Kmt2c* loss associates with, but does not enhance, expansion of *Ezh2*-deficient clones. (A) Peripheral blood gene knockout frequencies of an individual mouse (shCux1 mouse 1592) in which *Ezh2* and *Kmt2c* knockout trajectories are not correlated. Simple linear regression was performed to fit a line to the data, shown in dashes. (B) Same as in panel A, for an individual mouse (shCux1 mouse 159) with significantly correlated *Ezh2* and *Kmt2c* knockout (C) Bone marrow cells from the mouse in panel A (shCux1 mouse 1592) were plated in MethoCult M3434 methylcellulose, cultured for 1 week, and colonies derived from individual cells were genotyped. Each column is 1 colony. Blue shading denotes homozygous knockout, yellow denotes heterozygous knockout, and hatched lines denote the second allele harbored an in-frame indel that does not cause a frameshift. (D) Same as in panel C, for the mouse in panel B with no correlation between *Ezh2* and *Kmt2c* knockout (shCux1 mouse 159). (E) Box plots showing the maximum observed *Kmt2c* knockout values in the peripheral blood of mice receiving multiplex-edited shCtrl (left) and shCux1 (right) HSPCs. Each plot compares the maximum observed knockout between mice with and without significantly correlated *Ezh2* and *Kmt2c* knockout trajectories. Significance from a 2-tailed *t* test is shown. **$P < .01$. (F) The maximum observed *Ezh2* knockout values, same as in panel E. A 2-tailed *t* test was performed. CFU, colony-forming unit; Max, maximum.

Figure 3 (continued) over time in Veh-treated recipients of HSPCs transfected with RNPs targeting an intron of *Actb*, and ENU-treated recipients of multiplex-edited HSPCs. Veh-treated *Actb* mice were used as a comparison as ENU-treated mice died by 14 weeks. Data are plotted as mean + SD (n = 5 mice per experimental group for *Actb* recipients and n = 4 mice per experimental group for multiplex recipients). Significance from a 2-way ANOVA is shown. ***$P < .001$. (F) Spleen weight at time of euthanasia for the same mice as in panel E, with significance from a 2-tailed *t* test shown. ***$P < .001$. (G) CD45.2^{+} peripheral blood granulocytes (Gr1^{+}CD11b^{+}) and monocytes (Gr1^{−}CD11b^{+}) for the same mice as in panels E-F, with significance from 2-tailed *t* tests shown. *$P < .05$; **$P < .01$. (H) Bar plots of *Ezh2* knockout in recipients of multiplex-edited shCtrl cells (left) and shCux1 cells (right), arranged by survival time. Individual mouse ID numbers are provided on the x-axis. *Ezh2* knockout approaches 100%, consistent with biallelic gene loss, in aged recipients of shCux1 cells. CFU, colony-forming unit; ID, identity; RBC, red blood cell.
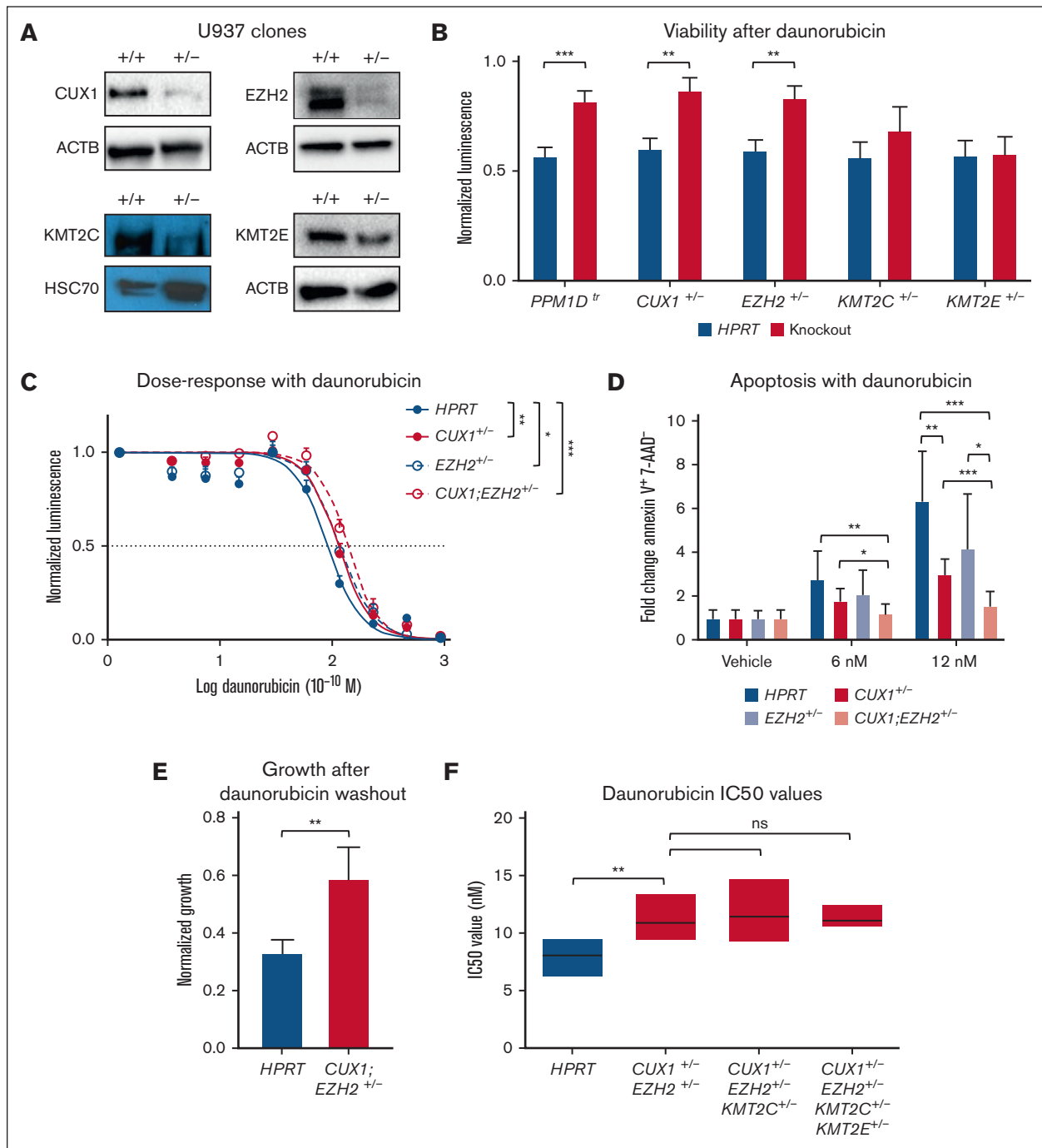
Figure 5. Combinatorial inactivation of *CUX1* and *EZH2* promotes resistance to the MN therapeutic daunorubicin. (A) U937 human myeloid leukemia cells were transfected with RNPs targeting *CUX1*, *EZH2*, *KMT2C*, or *KMT2E*, and clonal lines were derived harboring heterozygous knockout. Western blot validation is shown. Data are representative of n = 2 biological replicates. (B) Heterozygous knockout clones were plated with 3 nM daunorubicin or Veh for 72 hours, and viability was assessed via CellTiter-Glo luminescence. Cells transfected with RNPs targeting an intron of the *HPRT* gene were used as a wild-type control. Cells with a $PPM1D^{tr}$ were used as a positive control. Luminescence normalized to Veh-treated wells is shown. Two-tailed *t* tests were performed to compare normalized luminescence between 7q knockout cells and gHPRT control cells. Three biological replicates, each with 3 technical replicates, were performed. Data are plotted as mean + SEM. **$P < .01$; ***$P < .001$. (C) A *CUX1;EZH2*-double heterozygous U937 knockout clone was generated. *HPRT* control, single knockout, and double knockout cells were plated with increasing doses of daunorubicin (range, 0.375-96 nM) to generate a dose-response curve. Three biological replicates were performed, each with 3 technical replicates. Data are plotted as mean + SEM, and significance from 2-way ANOVA is shown. *$P < .05$; **$P < .01$; ***$P < .001$. (D) Apoptosis was measured by flow cytometry using Annexin-V at 2 doses of daunorubicin after 72 hours of treatment. Three biological replicates were performed, each with technical duplicates. Data are plotted as mean + SD, and significance from 1-way ANOVA with multiple corrections is shown. *$P < .05$; **$P < .01$; ***$P < .001$. (E) After 72-hour treatment with 6 nM daunorubicin, drug was washed out and equal numbers of Veh-treated and drug-treated *HPRT* and $CUX1;EZH2^{+/-}$ cells were reseeded in new culture plates. Cell growth in the drug-treated plates was normalized to that of Veh-treated plates for both *HPRT* and $CUX1;EZH2^{+/-}$.
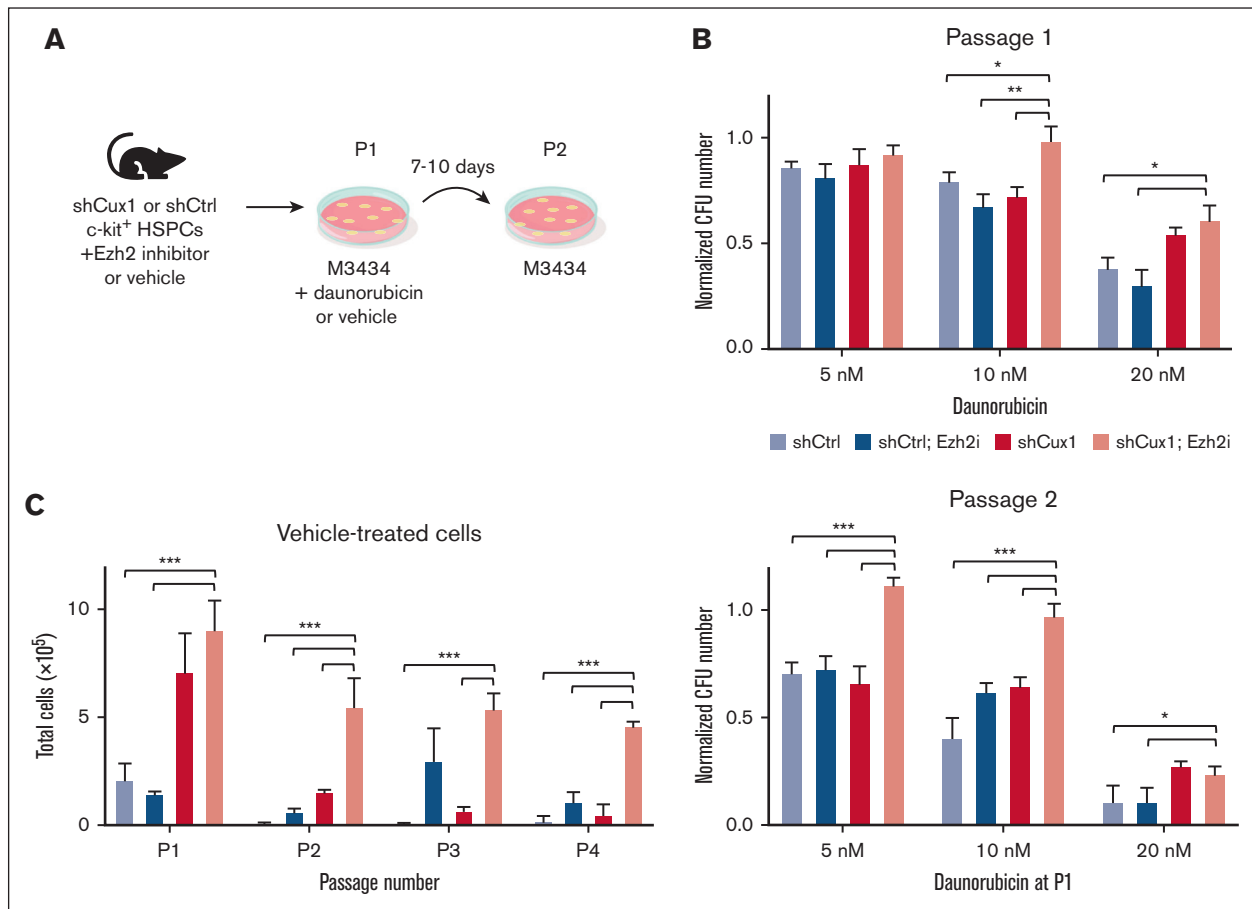
Figure 6. Combined *Cux1;Ezh2* deficiency promotes chemotherapy resistance in primary HSPCs. (A) Experimental schematic for primary cell drug resistance assays. shCtrl and shCux1 HSPCs were cultured with the EZH2 inhibitor tazemetostat (1 μM) or Veh for 5 days, with tazemetostat replenishment after 3 days. Cells were then plated in MethoCult M3434 methylcellulose with/without tazemetostat and daunorubicin. After 7 to 10 days, colonies were counted and reseeded to fresh M3434 for a second passage. Colonies were counted again after passage 2. Veh control was used for both tazemetostat and daunorubicin. (B) Clonogenic survival of HSPCs after passage 1 (top) and passage 2 (bottom). For each genotype, the number of colonies was normalized to Veh-treated control. Daunorubicin was present in passage 1. Three independent biological replicates with technical duplicates were performed. Data are plotted as mean + SEM, and significance from a 1-way ANOVA with multiple comparisons is shown. *$P < .05$; **$P < .01$; ***$P < .001$. (C) Total number of cells recovered at each passage from Veh-treated wells in panel B. Three independent biological replicates were performed, and 1 representative replicate is shown. Data are mean + SD, and significance from 1-way ANOVA with multiple comparisons is shown. ***$P < .001$.

component of induction therapy for AML and t-MN.[64] As controls, we used a clone with a neutral intronic indel of the *HPRT* gene and a clone with a *PPM1D* truncating mutation known to promote drug resistance.[60,65] We observed significantly increased viability with even single-copy loss of *CUX1* and *EZH2*, comparable with *PPM1D*-mutant cells, in response to daunorubicin (Figure 5B) and etoposide (supplemental Figure 5A).

To test combined loss of *CUX1* and *EZH2*, we generated a double-heterozygous clone (supplemental Figure 5B). *CUX1;*

EZH2^{+/−} cells showed a further increased 50% inhibitory concentration than either single gene deficiency for both daunorubicin and etoposide (Figure 5C; supplemental Figure 5C). Accordingly, *CUX1;EZH2*-deficient cells showed decreased apoptosis after culture with daunorubicin compared with *HPRT* cells and single heterozygotes (Figure 5D; supplemental Figure 5D). Even after washing out daunorubicin and reseeding equal numbers of viable cells, we observed significantly more growth from *CUX1; EZH2*-deficient cells (Figure 5E). Notably, daunorubicin 50% inhibitory concentration values did not increase in either a triple

Figure 5 (continued) Four biological replicates were performed. Data are plotted as mean + SD, and significance from a 2-tailed *t* test is shown. **$P < .01$. (F) Box plots of daunorubicin IC50 values from wild-type *HPRT*, *CUX1;EZH2*^{+/−} double heterozygous, *CUX1;EZH2;KMT2C*^{+/−} triple heterozygous, and *CUX1;EZH2;KMT2C;KMT2E*^{+/−} quadruple heterozygous cells. Data from n = 3 biological replicates are plotted, and significance from 2-tailed *t* tests is shown. **$P < .01$. IC50, 50% inhibitory concentration; ns, not significant; *PPM1D*[tr], *PPM1D* truncating mutation.
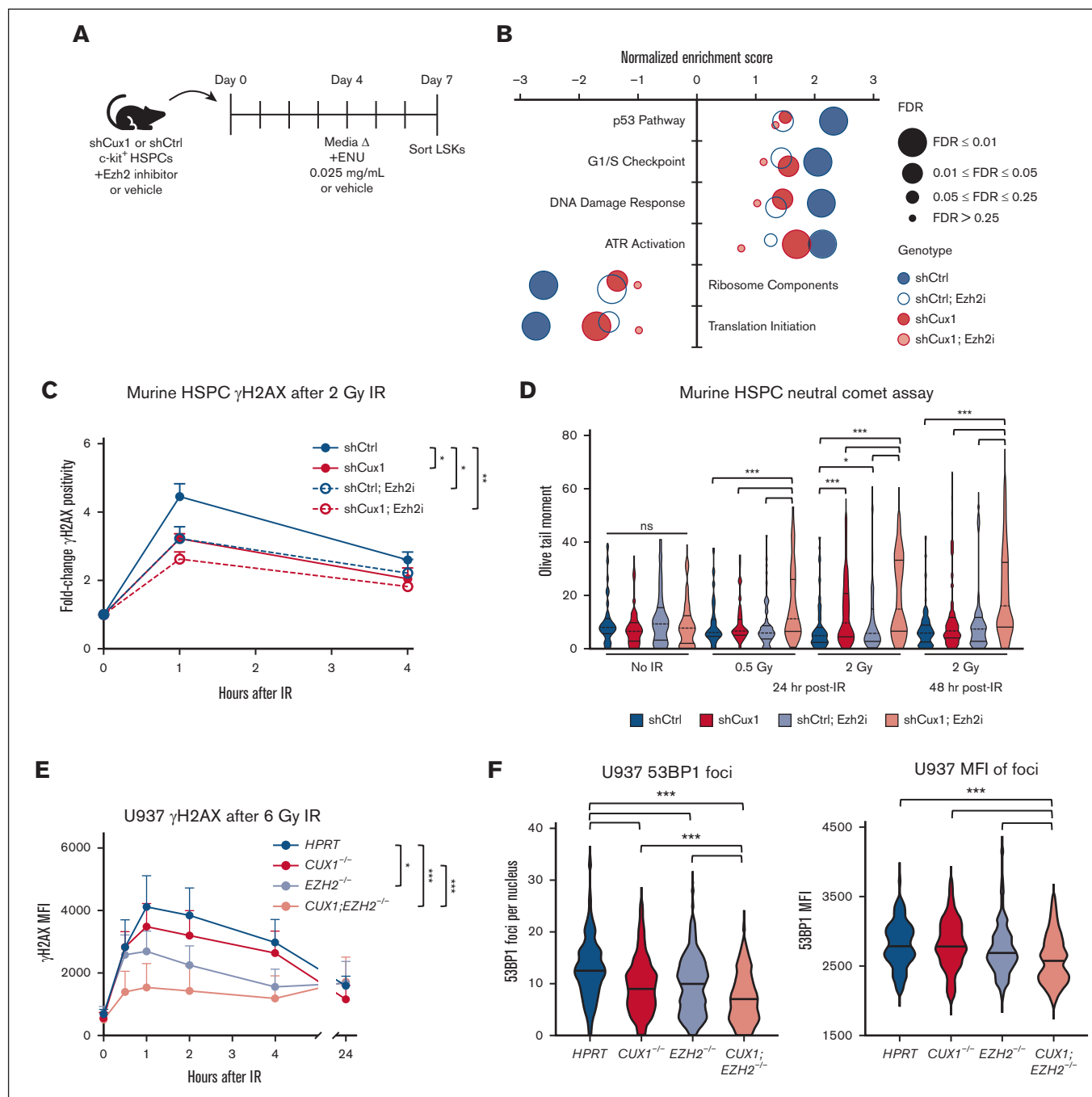
Figure 7. CUX1;EZH2-deficient cells have an impaired DDR. (A) Experimental scheme for RNA sequencing in the presence of ENU. shCtrl and shCux1 HSPCs were cultured with 1 μM tazemetostat or Veh for 4 days to mimic *Ezh2* loss. Media was replaced with fresh tazemetostat and 0.025 mg/mL ENU or Veh to induce DNA damage. After 72 hours of ENU treatment, LSK cells were sorted directly into TRIzol. RNA was extracted and prepared for sequencing. A wild-type shCtrl group without ENU treatment was included as a control. Three sets of biological replicates were sequenced. (B) Differential gene expression analysis was conducted with DE-Seq2, and gene rank lists were created for gene set enrichment analyses.[69] All genotypes were compared to shCtrl cells without ENU exposure. A multivariate plot showing the top positively and negatively enriched gene sets in shCtrl cells after ENU exposure is shown. Bubble color indicates genotype, and size denotes FDR. (C) shCtrl and shCux1 HSPCs were cultured for 5 days with 1 μM tazemetostat or Veh to mimic *Ezh2* loss, with tazemetostat replenishment after 3 days. Cells were then irradiated to induce DNA damage (2 Gy). γH2AX deposition was followed across 4 hours by intracellular flow cytometry, and the fold change of cells staining positive for γH2AX is plotted. Data (n = 4 biological replicates) are plotted as mean + SEM, and significance from 2-way ANOVA is shown. *$P < .05$; **$P < .01$. (D) shCtrl and shCux1 HSPCs were cultured for 5 days with 1 μM tazemetostat or Veh to mimic *Ezh2* loss, with tazemetostat replenishment after 3 days. Cells were then irradiated with 0.5 Gy or 2 Gy and neutral comet assays were performed. Nonirradiated cells were used as a control. Data (n = 3 biological replicates) are plotted as violin plots with quartiles, and 20 to 60 comets were analyzed per replicate. Total number of points are as follows: 110, 129, 79, and 84 (no IR); 86, 65, 72, and 103 (0.5 Gy); 100, 84, 128, and 133 (2 Gy, 24 hours); 120, 117, 118, and 174 (2 Gy, 48 hours), from left to right. Significance from Mann-Whitney *U* tests is shown. *$P < .05$; ***$P < .001$. (E) Clonal homozygous knockout U937 cells were irradiated to induce DNA damage (6 Gy), and γH2AX deposition was

heterozygote (*CUX1;EZH2;KMT2C*) or a quadruple heterozygote (Figure 5F).

Next, we assessed *Cux1* and *Ezh2* loss in chemotherapy resistance using primary shCtrl and shCux1 HSPCs. We plated cells in methylcellulose with the US Food and Drug Administration–approved EZH2 inhibitor, tazemetostat, to uniformly mimic *Ezh2* loss, and daunorubicin (Figure 6A; supplemental Figure 6A). Across 2 passages, tazemetostat-treated shCux1 cells demonstrated reduced sensitivity to multiple doses of daunorubicin as measured by colony numbers (Figure 6B).[66] Furthermore, we recovered significantly more cells at each passage from tazemetostat-treated shCux1 wells, suggesting increased progenitor proliferation (Figure 6C). Tazemetostat-treated shCux1 colonies were also significantly larger than treated shCtrl colonies, particularly at later passages (supplemental Figure 6B). We observed similar findings with GSK126, a second EZH2 inhibitor (supplemental Figure 6C-D). Thus, combined deficiency in CUX1 and EZH2 promotes daunorubicin resistance in primary HSPCs to a greater degree than either single gene deficiency.

Cux1;Ezh2-deficient cells have an abrogated DNA damage response after genotoxic stress

To determine whether combined *Cux1* and *Ezh2* deficiency induces expression of a unique set of genes or behaves additively, we performed RNA sequencing on shCtrl and shCux1 HSPCs transfected with gEzh2 or intronic gActb RNPs as a control. Differential gene expression analysis identified 1711 differentially expressed genes (false discovery rate of <0.05) across all 4 genotypes (supplemental Table 2). Hierarchical clustering analysis resolved clear gene signatures for *Cux1* and *Ezh2* loss, with derepression of PRC2 target genes in gEzh2 cells (supplemental Figure 7A).[67] *Cux1* and *Ezh2* were the top 2 downregulated genes, confirming the efficacy of our approach (supplemental Figure 7B). *Cux1;Ezh2*-deficient cells displayed both gene signatures, indicating additive transcriptional changes from combined deficiency. Accordingly, we noted *Cux1;Ezh2*-deficient cells, but not *Cux1;Kmt2c*-deficient cells, were more strongly enriched for patient-derived −7/del(7q) gene signatures than either single deficiency (supplemental Figure 7C-D).[68] *Cux1;Ezh2*-deficient cells were also enriched for a gene signature resembling *TP53* loss, which may contribute to the selective advantage we observed after genotoxic stress (supplemental Figure 7E).[69]

Our laboratory has also shown that CUX1 promotes epigenetic-driven DNA repair via interaction with the histone methyltransferase EHMT2/G9a.[26] Others have shown PRC2 directly interacts with EHMT2 and localizes to DNA breaks to deposit H3K27 methylation as part of the early DNA damage response (DDR).[54,55,70-72] Therefore, we hypothesized the selective advantage from *CUX1;EZH2* deficiency derives from further disruption to DNA damage recognition and repair. We performed a second RNA-sequencing experiment on shCtrl and shCux1 HSPCs with

ENU treatment to induce DNA damage (Figure 7A). We used ex vivo HSPCs rather than those from the ENU-treated animals to examine the immediate effects of *Cux1* and *Ezh2* loss and avoid heterogeneity from varying *Ezh2* editing efficiency. In these experiments, we uniformly suppressed EZH2 activity with tazemetostat before ENU addition. Differentially expressed gene analysis identified 3457 genes with false discovery rate of <0.01 (supplemental Table 3), and gene set enrichment analyses revealed striking differences between genotypes. The top enriched pathways in shCtrl cells after ENU were related to p53 activation and the DDR (Figure 7B). Pathways related to protein translation were negatively enriched, a known response to DNA damage.[73,74] Both *Cux1*- and *Ezh2*-deficient cells displayed reduced enrichment of these pathways, and *Cux1;Ezh2*-deficient cells had an abject failure to activate DDR pathways (Figure 7B). Blunted stress responses have been observed after inactivation of epigenetic regulators, including *EZH2*,[75] suggesting these compounding DDR defects may enable persistence of *Cux1;Ezh2*-deficient cells after genotoxic stress. We also observed enrichment for gene signatures associated with long-term HSCs[76] and decreased signatures for HSC differentiation[77] in *Cux1;Ezh2*-deficient cells that appeared driven by *Ezh2* loss (supplemental Figure 7F). These data suggest that the advantage from combined *Cux1;Ezh2* deficiency is multifaceted and includes increased stemness as well as additive defects to the DDR.

We previously showed that *Cux1*-deficient cells have reduced γH2AX deposition after irradiation (IR), an early step in the DDR[78]; indeed, cells with combined *Cux1;Ezh2* deficiency displayed a larger reduction in γH2AX deposition (Figure 7C). To assess whether the decrease in DNA damage recognition results in persistent, unrepaired damage, we performed neutral comet assays on irradiated HSPCs. Although control HSPCs resolved DNA damage within 24 hours after IR, cells deficient in *Cux1* or *Ezh2* displayed significantly elevated levels of DNA breaks, and *Cux1;Ezh2*-deficient HSPCs had even higher levels at 24 and 48 hours after IR (Figure 7D). Even a low-dose pulse of 0.5 Gy elevated DNA breaks in *Cux1;Ezh2*-deficient cells. We similarly observed significantly decreased γH2AX deposition in *CUX1;EZH2*-null U937 cells (Figure 7E; supplemental Figure 7G). Consequently, *CUX1;EZH2*-deficient cells have reduced 53BP1 foci number and intensity 1 hour after IR (Figure 7F), likely because of decreased EHMT2 and H3K27me2/3, both of which are required for efficient 53BP1 recruitment (supplemental Figure 7H).[26,79,80] Collectively, our data indicate CUX1 and EZH2 loss converges on DDR deregulation, which may enable mutant cells to persist through genotoxic stress and subsequently expand.

Discussion

Dissecting the pathogenesis of −7/del(7q) and other recurrent aneuploid events in cancer remains a challenge. Here we develop a model of del(7q) CH and drug resistance, taking an orthogonal

approach to identify candidate 7q genes most likely to interact with *CUX1* loss by leveraging publicly available CRISPR screen data and existing literature. Our multiplex knockout approach achieves population-level editing in primary HSCs in under 1 week, without viral plasmid delivery or antibiotic selection, and circumvents the lack of chromosomal synteny between humans and mice. Using this technique, we identify *CUX1* and *EZH2* as critical mediators of drug resistance and clonal expansion that converge on deregulation of the DDR. This work supports the concept of 7q as a contiguous gene syndrome region containing multiple TSGs, similar to contiguous regions identified on 5q and 8p.[81-84]

KMT2C mutations have been identified in primary AML and relapsed pediatric AML,[46,62] and *Kmt2c*$^{+/-}$ HSCs expand after exposure to alkylating agents.[45] In our model, *Kmt2c* loss associates with *Cux1* deficiency but the effects on expansion are variable (Figure 1H). Although *Kmt2c* loss trend toward promoting expansion in the setting of combined *Cux1*;*Ezh2* deficiency (Figure 4E-F), our data demonstrate a stronger interaction between *Cux1* and *Ezh2* loss. We also note that loss of multiple 7q genes is insufficient to fully rescue the engraftment defects from *Kmt2e* loss, although there were notable examples in which *Kmt2e* was co-mutated with *Ezh2* (Figure 3A-C).[48,53] Because all 4 of these 7q genes have been implicated in DNA damage repair, there may be functional redundancy between deletion phenotypes with *Cux1* and *Ezh2* loss possessing the highest penetrance.

Patient-derived monosomy 7 cells display downregulated DNA damage checkpoint and apoptosis genes,[85] and our RNA sequencing revealed a profound failure of *Cux1*;*Ezh2*-deficient cells to activate the DDR after ENU exposure (Figure 7B). CUX1 may recruit PRC2/EZH2 to sites of DNA damage via G9a/EHMT2 to enable deposition of H3K27me3, an early step in the DDR.[26,54,71] EZH2 inhibition also downregulates DDR genes via decreased methylation of activating pioneer transcription factors.[86] Thus, the compounding deregulation of the early DDR we observed may be multifaceted, with both transcriptional and nontranscriptional origins (Figure 7B-E).

CH variants in DDR genes are selected for after genotoxic stress, likely because of increased survival of mutant cells.[60,65,87] Variants in epigenetic regulators are also positively selected for, likely via increased self-renewal as well as blunted responses to external stressors.[75,88] Our work positions *CUX1* and *EZH2*, which are themselves mutated in CH,[17,89-92] at the intersection of these pathways promoting increased survival (Figure 2D; supplemental Figure 3D) and stemness (Figure 6C; supplemental Figure 7F). Even in absence of chemotherapeutic pressure there may be a synergistic role for *CUX1* and *EZH2* loss (Figure 3A-C). Whether other elements of −7/del(7q) biology contribute to pathogenicity, including altered splicing from *LUC7L2* deletions[93,94] and cytokine hypersensitivity from *SAMD9*/*SAMD9L* loss,[95] remains unknown. Future studies characterizing del(7q) should be performed with combined *CUX1* and *EZH2* deficiency as a foundation.

Authorship

Contribution: M.R.M.J. designed and performed experiments, analyzed data, and wrote the manuscript; A.S. assisted with the multiplex knockout transplants and edited the manuscript; T.C.M. assisted with cell sorting, mouse transplants, and RNA-sequencing analysis; R.M. assisted with immunofluorescence micrographs; Y.X. assisted with neutral comet assays; M.K.I. assisted with dose-response assays; H.B. assisted with secondary transplants; H.S.N and B.H. assisted with data mining; J.A. assisted with DNA extraction for Sanger sequencing; N.A. and S.K. provided conceptual and technical advice; S.K.G. assisted with hematoxylin and eosin imaging and analysis; and M.E.M. conceived the experiments, interpreted data, and edited the manuscript.

Conflict-of-interest disclosure: The authors declare no competing financial interests.

ORCID profiles: M.R.M.J., 0000-0001-7632-8625; T.C.M., 0000-0002-7074-9610; Y.X., 0000-0002-8909-0270; M.K.I., 0000-0003-3724-5338; H.S.N., 0009-0002-5654-320X; B.H., 0000-0001-8970-3201; S.K.G., 0000-0003-0716-8730; M.E.M., 0000-0002-8260-3598.

Correspondence: Megan E. McNerney, Department of Pathology, The University of Chicago, 5128 Knapp Center for Biomedical Discovery, 900 East 57th St, Chicago, IL 60637; email: megan.mcnerney@uchospitals.edu.

References

1. Weaver BAA, Cleveland DW. Does aneuploidy cause cancer? *Curr Opin Cell Biol*. 2006;18:658-667.

2. Chunduri NK, Storchová Z. The diverse consequences of aneuploidy. *Nat Cell Biol*. 2019;21:54-62.

3. Donnelly N, Passerini V, Dürrbaum M, Stingele S, Storchová Z. HSF1 deficiency and impaired HSP90-dependent protein folding are hallmarks of aneuploid human cells. *EMBO J*. 2014;33:2374-2387.

4. Williams BR, Prabhu VR, Hunter KE, et al. Aneuploidy affects proliferation and spontaneous immortalization in mammalian cells. *Science*. 2008;322:703-709.

5. Vasudevan A, Schukken KM, Sausville EL, et al. Aneuploidy as a promoter and suppressor of malignant growth. *Nat Rev Cancer*. 2021;21:89-103.

6. Kotini AG, Chang CJ, Boussaad I, et al. Functional analysis of a chromosomal deletion associated with myelodysplastic syndromes using isogenic human induced pluripotent stem cells. *Nat Biotechnol*. 2015;33:646-655.

7. McNerney ME, Godley LA, Le Beau MM. Therapy-related myeloid neoplasms: when genetics and environment collide. *Nat Rev Cancer*. 2017;17:513-527.

8. Wong JC, Weinfurtner KM, Alzamora Mdel P, et al. Functional evidence implicating chromosome 7q22 haploinsufficiency in myelodysplastic syndrome pathogenesis. *eLife*. 2015;4:e07839.

9. Schwartz JR, Ma J, Lamprecht T, et al. The genomic landscape of pediatric myelodysplastic syndromes. *Nat Commun*. 2017;8:1557.

10. Papaemmanuil E, Döhner H, Campbell PJ. Genomic classification in acute myeloid leukemia. *N Engl J Med*. 2016;375:900-901.

11. Haase D. Cytogenetic features in myelodysplastic syndromes. *Ann Hematol*. 2008;87:515-526.

12. Smith SM, Le Beau MM, Huo D, et al. Clinical-cytogenetic associations in 306 patients with therapy-related myelodysplasia and myeloid leukemia: the University of Chicago series. *Blood*. 2003;102:43-52.

13. Arber DA, Orazi A, Hasserjian RP, et al. International Consensus Classification of myeloid neoplasms and acute leukemias: integrating morphologic, clinical, and genomic data. *Blood*. 2022;140:1200-1228.

14. Khoury JD, Solary E, Abla O, et al. The 5th edition of the World Health Organization classification of haematolymphoid tumours: myeloid and histiocytic/dendritic neoplasms. *Leukemia*. 2022;36:1703-1719.

15. Machiela MJ, Zhou W, Sampson JN, et al. Characterization of large structural genetic mosaicism in human autosomes. *Am J Hum Genet*. 2015;96:487-497.

16. Loh P-R, Genovese G, Handsaker RE, et al. Insights into clonal haematopoiesis from 8,342 mosaic chromosomal alterations. *Nature*. 2018;559:350-355.

17. Gao T, Ptashkin R, Bolton KL, et al. Interplay between chromosomal alterations and gene mutations shapes the evolutionary trajectory of clonal hematopoiesis. *Nat Commun*. 2021;12:338.

18. Saiki R, Momozawa Y, Nannya Y, et al. Combined landscape of single-nucleotide variants and copy number alterations in clonal hematopoiesis. *Nat Med*. 2021;27:1239-1249.

19. Takahashi K, Wang F, Kantarjian H, et al. Copy number alterations detected as clonal hematopoiesis of indeterminate potential. *Blood Adv*. 2017;1:1031-1036.

20. Takahashi K, Wang F, Kantarjian H, et al. Preleukaemic clonal haemopoiesis and risk of therapy-related myeloid neoplasms: a case-control study. *Lancet Oncol*. 2017;18:100-111.

21. Inaba T, Honda H, Matsui H. The enigma of monosomy 7. *Blood*. 2018;131:2891-2898.

22. Jotte MRM, McNerney ME. The significance of CUX1 and chromosome 7 in myeloid malignancies. *Curr Opin Hematol*. 2022;29:92-102.

23. Mori M, Kubota Y, Durmaz A, et al. Genomics of deletion 7 and 7q in myeloid neoplasm: from pathogenic culprits to potential synthetic lethal therapeutic targets. *Leukemia*. 2023;37:2082-2093.

24. McNerney ME, Brown CD, Wang X, et al. CUX1 is a haploinsufficient tumor suppressor gene on chromosome 7 frequently inactivated in acute myeloid leukemia. *Blood*. 2013;121:975-983.

25. An N, Khan S, Imgruet MK, et al. Gene dosage effect of CUX1 in a murine model disrupts HSC homeostasis and controls the severity and mortality of MDS. *Blood*. 2018;131:2682-2697.

26. Imgruet MK, Khan S, Imgruet MK, et al. Loss of a 7q gene, CUX1, disrupts epigenetically driven DNA repair and drives therapy-related myeloid neoplasms. *Blood*. 2021;138:790-805.

27. Supper E, Rudat S, Iyer V, et al. Cut-like homeobox 1 (CUX1) tumor suppressor gene haploinsufficiency induces apoptosis evasion to sustain myeloid leukemia. *Nat Commun*. 2021;12(1):2482.

28. Olivieri M, Cho T, Álvarez-Quilón A, et al. A genetic map of the response to DNA damage in human cells. *Cell*. 2020;182:481-496.e21.

29. Findlay S, Heath J, Luo VM, et al. SHLD2/FAM35A co-operates with REV7 to coordinate DNA double-strand break repair pathway choice. *EMBO J*. 2018;37:e100158.

30. Wijdeven RH, Heath J, Luo VM, et al. Genome-wide identification and characterization of novel factors conferring resistance to topoisomerase II poisons in cancer. *Cancer Res*. 2015;75:4176-4187.

31. Goodspeed A, Jean A, Costello JC. A whole-genome CRISPR screen identifies a role of MSH2 in cisplatin-mediated cell death in muscle-invasive bladder cancer. *Eur Urol*. 2019;75:242-250.

32. He YJ, Meghani K, Caron MC, et al. DYNLL1 binds to MRE11 to limit DNA end resection in BRCA1-deficient cells. *Nature*. 2018;563:522-526.

33. Liu C, Banister CE, Buckhaults PJ. Spindle assembly checkpoint inhibition can resensitize p53-null stem cells to cancer chemotherapy. *Cancer Res.* 2019;79:2392-2403.

34. Huang D, Savage SR, Calinawan AP, et al. A highly annotated database of genes associated with platinum resistance in cancer. *Oncogene.* 2021;40:6395-6405.

35. Awah CU, Chen L, Bansal M, et al. Ribosomal protein S11 influences glioma response to TOP2 poisons. *Oncogene.* 2020;39:5068-5081.

36. Wang T, Wei JJ, Sabatini DM, Lander ES. Genetic screens in human cells using the CRISPR-Cas9 system. *Science.* 2014;343:80-84.

37. Oughtred R, Rust J, Chang C, et al. The BioGRID database: a comprehensive biomedical resource of curated protein, genetic, and chemical interactions. *Protein Sci Publ Protein Soc.* 2021;30:187-200.

38. Liberzon A, Subramanian A, Pinchback R, Thorvaldsdóttir H, Tamayo P, Mesirov JP. Molecular signatures database (MSigDB) 3.0. *Bioinforma Oxf Engl.* 2011;27:1739-1740.

39. Gundry MC, Brunetti L, Lin A, et al. Highly efficient genome editing of murine and human hematopoietic progenitor cells by CRISPR/Cas9. *Cell Rep.* 2016;17:1453-1461.

40. Pasini D, Bracken AP, Jensen MR, Denchi EL, Helin K. Suz12 is essential for mouse development and for EZH2 histone methyltransferase activity. *EMBO J.* 2004;23:4061-4071.

41. Piunti A, Shilatifard A. The roles of Polycomb repressive complexes in mammalian development and cancer. *Nat Rev Mol Cell Biol.* 2021;22:326-345.

42. Göllner S, Oellerich T, Agrawal-Singh S, et al. Loss of the histone methyltransferase EZH2 induces resistance to multiple drugs in acute myeloid leukemia. *Nat Med.* 2017;23:69-78.

43. Hu D, Gao X, Morgan MA, et al. The MLL3/MLL4 branches of the COMPASS family function as major histone H3K4 monomethylases at enhancers. *Mol Cell Biol.* 2013;33:4745-4754.

44. Meeks JJ, Shilatifard A. Multiple roles for the MLL/COMPASS family in the epigenetic regulation of gene expression and in cancer. *Annu Rev Cancer Biol.* 2017;1:425-446.

45. Chen R, Okeyo-Owuor T, Patel RM, et al. Kmt2c mutations enhance HSC self-renewal capacity and convey a selective advantage after chemotherapy. *Cell Rep.* 2021;34:108751.

46. McNeer NA, Philip J, Geiger H, et al. Genetic mechanisms of primary chemotherapy resistance in pediatric acute myeloid leukemia. *Leukemia.* 2019;33:1934-1943.

47. Heuser M, Yap DB, Leung M, et al. Loss of MLL5 results in pleiotropic hematopoietic defects, reduced neutrophil immune function, and extreme sensitivity to DNA demethylation. *Blood.* 2009;113:1432-1443.

48. Madan V, Madan B, Brykczynska U, et al. Impaired function of primitive hematopoietic cells in mice lacking the mixed-lineage-leukemia homolog MLL5. *Blood.* 2009;113:1444-1454.

49. Zhang Y, Wong J, Klinger M, et al. MLL5 contributes to hematopoietic stem cell fitness and homeostasis. *Blood.* 2009;113:1455-1463.

50. Damm F, Oberacker T, Thol F, et al. Prognostic importance of histone methyltransferase MLL5 expression in acute myeloid leukemia. *J Clin Oncol.* 2011;29:682-689.

51. Chang A, Liu L, Ashby JM, et al. Recruitment of KMT2C/MLL3 to DNA damage sites mediates DNA damage responses and regulates PARP inhibitor sensitivity in cancer. *Cancer Res.* 2021;81:3358-3373.

52. Rampias T, Karagiannis D, Avgeris M, et al. The lysine-specific methyltransferase KMT2C/MLL3 regulates DNA repair components in cancer. *EMBO Rep.* 2019;20:e46821.

53. Tasdogan A, Kumar S, Allies G, et al. DNA damage-induced HSPC malfunction depends on ROS accumulation downstream of IFN-1 signaling and bid mobilization. *Cell Stem Cell.* 2016;19:752-767.

54. Campbell S, Ismail IH, Young LC, Poirier GG, Hendzel MJ. Polycomb repressive complex 2 contributes to DNA double-strand break repair. *Cell Cycle.* 2013;12:2675-2683.

55. Lutze J, Wolfgeher D, Kron SJ. Global epigenetic analysis reveals H3K27 methylation as a mediator of double strand break repair. *bioRxiv.* Preprint posted online 20 September 2021. https://doi.org/10.1101/2021.09.20.461136

56. Hoadley KA, Yau C, Hinoue T, et al. Cell-of-origin patterns dominate the molecular classification of 10,000 tumors from 33 types of cancer. *Cell.* 2018;173:291-304.e6.

57. Yuan Y, Zhou L, Miyamoto T, et al. AML1-ETO expression is directly involved in the development of acute myeloid leukemia in the presence of additional mutations. *Proc Natl Acad Sci U S A.* 2001;98:10398-10403.

58. Kurtz KJ, Conneely SE, O'Keefe M, Wohlan K, Rau RE. Murine models of acute myeloid leukemia. *Front Oncol.* 2022;12:854973.

59. Challen GA, Boles N, Lin KK, Goodell MA. Mouse hematopoietic stem cell identification and analysis. *Cytometry Part J Int Soc Anal Cytol.* 2009;75(1):14-24.

60. Kahn JD, Miller PG, Silver AJ, et al. PPM1D-truncating mutations confer resistance to chemotherapy and sensitivity to PPM1D inhibition in hematopoietic cells. *Blood.* 2018;132:1095-1105.

61. Jerez A, Sugimoto Y, Makishima H, et al. Loss of heterozygosity in 7q myeloid disorders: clinical associations and genomic pathogenesis. *Blood.* 2012;119:6109-6117.

62. Halik A, Tilgner M, Silva P, et al. Genomic characterization of acute myeloid leukemia with aberrations of chromosome 7: a multinational cohort of 523 patients. *Blood*. 2023;142(suppl 1):63.

63. Kakinuma S, Nishimura M, Kubo A, et al. Frequent retention of heterozygosity for point mutations in p53 and Ikaros in N-ethyl-N-nitrosourea-induced mouse thymic lymphomas. *Mutat Res*. 2005;572:132-141.

64. Döhner H, Wei AH, Appelbaum FR, et al. Diagnosis and management of AML in adults: 2022 recommendations from an international expert panel on behalf of the ELN. *Blood*. 2022;140:1345-1377.

65. Hsu JI, Dayaram T, Tovy A, et al. PPM1D mutations drive clonal hematopoiesis in response to cytotoxic chemotherapy. *Cell Stem Cell*. 2018;23: 700-713.e6.

66. Guryanova OA, Shank K, Spitzer B, et al. DNMT3A mutations promote anthracycline resistance in acute myeloid leukemia via impaired nucleosome remodeling. *Nat Med*. 2016;22:1488-1495.

67. Mochizuki-Kashio M, Aoyama K, Sashida G, et al. Ezh2 loss in hematopoietic stem cells predisposes mice to develop heterogeneous malignancies in an Ezh1-dependent manner. *Blood*. 2015;126:1172-1183.

68. Helsmoortel HH, Bresolin S, Lammens T, et al. LIN28B overexpression defines a novel fetal-like subgroup of juvenile myelomonocytic leukemia. *Blood*. 2016;127:1163-1172.

69. Subramanian A, Tamayo P, Mootha VK, et al. Gene set enrichment analysis: a knowledge-based approach for interpreting genome-wide expression profiles. *Proc Natl Acad Sci U S A*. 2005;102:15545-15550.

70. Mozzetta C, Pontis J, Fritsch L, et al. The histone H3 lysine 9 methyltransferases G9a and GLP regulate polycomb repressive complex 2-mediated gene silencing. *Mol Cell*. 2014;53:277-289.

71. O'Hagan HM, Mohammad HP, Baylin SB. Double strand breaks can initiate gene silencing and SIRT1-dependent onset of DNA methylation in an exogenous promoter CpG island. *PLoS Genet*. 2008;4:e1000155.

72. O'Hagan HM, Wang W, Sen S, et al. Oxidative damage targets complexes containing DNA methyltransferases, SIRT1, and polycomb members to promoter CpG islands. *Cancer Cell*. 2011;20:606-619.

73. Halim VA, García-Santisteban I, Warmerdam DO, et al. Doxorubicin-induced DNA damage causes extensive ubiquitination of ribosomal proteins associated with a decrease in protein translation. *Mol Cell Proteomics*. 2018;17:2297-2308.

74. Silva E, Ideker T. Transcriptional responses to DNA damage. *DNA Repair*. 2019;79:40-49.

75. Loukas I, Simeoni F, Milan M, et al. Selective advantage of epigenetically disrupted cancer cells via phenotypic inertia. *Cancer Cell*. 2023;41(1):70-87. e14.

76. Ivanova NB, Dimos JT, Schaniel C, Hackney JA, Moore KA, Lemischka IR. A stem cell molecular signature. *Science*. 2002;298:601-604.

77. Agrawal A, Balci H, Hanspers K, et al. WikiPathways 2024: next generation pathway database. *Nucleic Acids Res*. 2024;52:D679-D689.

78. Kinner A, Wu W, Staudt C, Iliakis G. Gamma-H2AX in recognition and signaling of DNA double-strand breaks in the context of chromatin. *Nucleic Acids Res*. 2008;36:5678-5694.

79. Zhang Y, Chang JF, Sun J, et al. Histone H3K27 methylation modulates the dynamics of FANCD2 on chromatin to facilitate NHEJ and genome stability. *J Cell Sci*. 2018;131:jcs215525.

80. Ginjala V, Rodriguez-Colon L, Ganguly B, et al. Protein-lysine methyltransferases G9a and GLP1 promote responses to DNA damage. *Sci Rep*. 2017;7: 16613.

81. Ebert BL, Pretz J, Bosco J, et al. Identification of RPS14 as a 5q- syndrome gene by RNA interference screen. *Nature*. 2008;451:335-339.

82. Starczynowski DT, Kuchenbauer F, Argiropoulos B, et al. Identification of miR-145 and miR-146a as mediators of the 5q- syndrome phenotype. *Nat Med*. 2010;16:49-58.

83. Stoddart A, Wang J, Fernald AA, Karrison T, Anastasi J, Le Beau MM. Cell intrinsic and extrinsic factors synergize in mice with haploinsufficiency for Tp53, and two human del(5q) genes, Egr1 and Apc. *Blood*. 2014;123:228-238.

84. Xue W, Kitzing T, Roessler S, et al. A cluster of cooperating tumor-suppressor gene candidates in chromosomal deletions. *Proc Natl Acad Sci U S A*. 2012;109:8212-8217.

85. Zhao X, Gao S, Wu Z, et al. Single-cell RNA-seq reveals a distinct transcriptome signature of aneuploid hematopoietic cells. *Blood*. 2017;130:2762-2773.

86. Liao Y, Chen CH, Xiao T, et al. Inhibition of EZH2 transactivation function sensitizes solid tumors to genotoxic stress. *Proc Natl Acad Sci U S A*. 2022; 119:e2105898119.

87. Wong TN, Miller CA, Jotte MRM, et al. Cellular stressors contribute to the expansion of hematopoietic clones of varying leukemic potential. *Nat Commun*. 2018;9:455.

88. Challen GA, Goodell MA. Clonal hematopoiesis: mechanisms driving dominance of stem cell clones. *Blood*. 2020;136:1590-1598.

89. Jaiswal S, Fontanillas P, Flannick J, et al. Age-related clonal hematopoiesis associated with adverse outcomes. *N Engl J Med*. 2014;371:2488-2498.

90. Yoshizato T, Dumitriu B, Hosokawa K, et al. Somatic mutations and clonal hematopoiesis in aplastic anemia. *N Engl J Med*. 2015;373:35-47.

91. Zink F, Stacey SN, Norddahl GL, et al. Clonal hematopoiesis, with and without candidate driver mutations, is common in the elderly. *Blood*. 2017;130: 742-752.

92. Robertson NA, Latorre-Crespo E, Terradas-Terradas M, et al. Longitudinal dynamics of clonal hematopoiesis identifies gene-specific fitness effects. *Nat Med*. 2022;28:1439-1446.

93. Daniels NJ, Hershberger CE, Gu X, et al. Functional analyses of human LUC7-like proteins involved in splicing regulation and myeloid neoplasms. *Cell Rep*. 2021;35:108989.

94. Jourdain AA, Begg BE, Mick E, et al. Loss of LUC7L2 and U1 snRNP subunits shifts energy metabolism from glycolysis to OXPHOS. *Mol Cell*. 2021; 81:1905-1919.e12.

95. Nagamachi A, Matsui H, Asou H, et al. Haploinsufficiency of SAMD9L, an endosome fusion facilitator, causes myeloid malignancies in mice mimicking human diseases with monosomy 7. *Cancer Cell*. 2013;24:305-317.